Preparation and Morphological Evolution of Heterophasic PP-EP/EVA/Organoclay Nanocomposites: Effect of the Nanoclay Organic Modifier

M. Valera-Zaragoza,[1] E. Ramírez-Vargas,[1] F. J. Medellín-Rodríguez[2]

[1]*Centro de Investigación en Química Aplicada, Blvd. Enrique Reyna 140, Saltillo, Coahuila 25100, México*
[2]*CIEP-FCQ, UASLP, Av. Dr. Manuel Nava 6, Zona Universitaria, San Luis Potosi, S.L.P. 78210, México*

Received 1 May 2006; accepted 18 June 2007
DOI 10.1002/app.27858
Published online 1 February 2008 in Wiley InterScience (www.interscience.wiley.com).

ABSTRACT: A study is presented on the morphological effects caused by the nanoclay organic modifier and the nanoclay concentration. This was made under previously determined compatibility conditions of heterophasic polypropylene copolymers (PP-EP)/poly(ethylene vinyl acetate) (EVA)/organoclay nanocomposites. The nanocomposites were prepared using the fluidity of the EVA phase to disperse the nanoclay platelets. Therefore, no additional compatibilizer was used to achieve the clay dispersion. Two organoclays were used with different characteristics and polarity of the substituent groups. Transmission electron microscopy and X-ray diffraction results first indicated that two hydrogenated tallow modifiers are more effective than one to enhance nanoclay exfoliation. Thermogravimetric studies indicated a low probability of thermal degradation of the nanoclay modifiers and as a consequence of their effect on the layer–layer exfoliation. Molecular simulations were made with the purpose to study additional factors affecting exfoliation. The introduction of nanoclay, within the compatibility conditions of the PP-EP/EVA system, was also studied. It was determined that the system preserved its original morphology and that the silicate layers were hosted by the EVA domains. The crystallization characteristics of the PP-EP/EVA mixtures indicated a gradual evolution of the overall crystalline structures depending on the EVA content. In the case of the ternary nanocomposites PP-EP/EVA/nanoclay, the β crystalline structure was partially formed, although it decreased with increasing nanoclay content. J Appl Polym Sci 108: 1986–1994, 2008

Key words: PP-EP/EVA blends; nanostructured polymers; nanoclays

INTRODUCTION

Silicate-layered nanocomposites are materials with improved properties depending on the dispersion of the nanoclay layers within the polymeric matrix. Molecular characteristics of the organic modifier attached to the clay, and also polarity of the polymer, have been reported to influence the desired nanoclay exfoliated condition.[1–3] However, in polymers with low polarity only the chemical modification of the polymer itself has proven to facilitate the formation of exfoliated nanostructured composites. This is the case of polypropylene, a polymer that does not allow favorable interactions with treated nanoclays. Polymer/clay interactions have been in some cases improved with maleic anhydride-grafted polypropylene (PP-MA),[4–6] and through iPP functionalization.[7] Ristolainen et al.[8] compared hydroxyl-functionalized polypropylene with a commercial, maleic anhydride functionalized, polypropylene in terms of clay exfoliation. The results indicated an intercalated-exfoliated morphology in the hydroxyl-functionalized polypropylene although they were not better than those observed in the maleic anhydride polymeric system. Mani et al.[9] used a titanate coupling agent to improve compatibility of the nanoclay particles with polypropylene although the authors reported the formation of intercalated structures rather than exfoliated layers. Gahleitner et al.[10] prepared a complex ternary system of polypropylene/polyamide 6/organoclay using compatibilizers of polypropylene and styrene elastomer. Both components were grafted with maleic anhydride and the mechanical properties of products were determined. The results indicated preferential affinity of nanoclay by the polyamide phase, which resulted in minimal changes in mechanical properties.

Previous studies on the dispersion of nanoclays in EVA, without the requirement of compatibilizers, have also been reported.[11–13] The results indicated

Correspondence to: F. J. Medellín-Rodríguez (francmr@uaslp.mx) or E. Ramírez-Vargas (evargas@ciqa.mx).

Contract grant sponsor: National Research Council of Science and Technology (CONACYT) of Mexico; contract grant numbers: 43983/A-1, U40177-Y.

that the partial polarity of the vinyl acetate (VA) groups in EVA allow favorable interactions with the clay nanolayers.[11] In the preparation of EVA nanocomposites, the clay organic modifier has also been an important factor. For example, Chaudhary et al.[14] obtained better intercalation in EVA nanocomposites when they used an organic modifier with polar groups instead of an organic modifier with aliphatic chains. In a different study, Peeterbroeck et al.[15] reported the effects of different commercial clays on the morphology and on the thermal and mechanical properties of EVA. The authors obtained intercalated and exfoliated structures depending on the polarity of the organic modifier. In this case, nanocomposites based on Cloisite 30B presented the highest exfoliation. The effect was assigned to interactions between the acetate part of EVA and the hydroxyethyl ammonium cations in Cloisite 30B. On the other hand, it was also reported[16,17] that the d_{001} reflection peak in the X-ray diffraction patterns shifted toward higher 2θ values, indicating a smaller exfoliation of the nanolayers in PP/Cloisite 30B,[16] and in EVA-*g*-MA/Cloisite 30B composites.[17] Coincident with these last studies, Zanetti et al.[18] used montmorillonite exchanged with octadecyl ammonium in EVA. They observed a decrease in exfoliation and assigned it to the partial thermal decomposition and volatilization of the modifier during blending.

In one of our recent studies with complex copolymeric systems,[19] where a range of compatibility was previously determined,[20,21] we reported increments in the thermal stability of the PP-EP/(EVA/C20A) ternary system as a results of layer exfoliation in EVA. In this particular case no compatibilizer was used and the hypothesis was taken that the elastomeric EVA phase provided the low viscosity component in the blend so as to promote nanoclay exfoliation. As a natural consequence, the main objective of the present study was to determine effects, mainly morphological, which were caused by the nature of the clay organic modifier, the concentration of nanoclay, and the compatibility conditions.

EXPERIMENTAL

Materials

A heterophasic polypropylene-(ethylene propylene) (PP-EP) copolymer from Montell Polyolefins (Profax 7523) was used as the reference copolymer. It had a melt flow index (MFI) of 4.0 dg/min, a density of 0.9 g/cm^3, a number-average molecular-weight (M_n) of 50,810 g/g-mol, a weight-average-molecular-weight (M_w) of 238,600 g/g-mol, and a polydispersity index (PI) of 4.7. The ethylene content was 8 wt %. The ethylene vinyl acetate (EVA) copolymer (Elvax 3174) was obtained from Du Pont with the following characteristics: Melt flow index (MFI) 8.0 dg/min, density 0.94 g/cm^3; number-average molecular weight (M_n) 22,460 g/g-mol; weight-average molecular weight (M_w) 137,550 g/g-mol, and PI 6.1. The vinyl acetate (VA) content was 18 wt %. Closites 20A and 30B were obtained from Southern Clay. Cloisite 20A was organically modified nanoclay with dimethyl dihydrogenated tallow quaternary ammonium chloride (two hydrogenated tallows). Cloisite 30B was organically modified nanoclay with methyl tallow, bis-2-hydroxyethyl, quaternary ammonium chloride (one hydrogenated tallow).

Nanocomposites preparation

A Werner and Pfleiderer corotating twin screw extruder (ZSK-30) was used to obtain the required nanocomposites. Before blending, all polymers and organoclays were dried at 60°C for 3 h. Mixtures of EVA and organoclay were prepared with 2, 4, 6, 8, and 10 wt % clay in a first blending cycle at 130°C. These preparations were blended with the PP-EP heterophasic copolymer in a second blending cycle at 190°C. Blends of the ternary system were prepared with EVA concentrations of 10, 20, 40, 60, and 70 wt %. The organoclay concentration was calculated on the basis of the EVA content, assuming that during blending there were only interactions with EVA in accordance with

$$\text{wt \% Clay}_{\text{system}} = \frac{\text{wt \% EVA} \times \text{wt \% Clay}_{\text{EVA}}}{100} \quad (1)$$

where wt % EVA corresponds to the EVA concentration and wt % Clay$_{\text{EVA}}$ indicates the clay content in EVA. Nanocomposites were pelletized and then injection molded in a Battenfeld injection molding machine (BA 750 CDK). Processing temperatures between 120 and 140°C were used in the case of the EVA/Clay hybrids and from 180 to 200°C in the case of PP-EP/(EVA/C20A) nanocomposites.

Transmission electron microscopy

Ultra-thin sections of samples were obtained using an Ultracut Leica EMFCS ultra microtome equipped with diamond knife. Transmission electron microscopy images were obtained from these specimens using a JEOL 1200-EXII transmission electron microscope with an acceleration voltage of 60 kV. The obtained negatives were scanned in a Duoscan T2500 AGFA scanner using the Fotolook 32 V3.60.0 software from Adobe Photoshop.

Wide angle X-ray diffraction

X-ray diffraction patterns were obtained in a Siemens D-500 diffractometer using a Ni-filtered Cu Kα radiation generator with an intensity of 25 mA and an accelerating voltage of 35 kV. The diffraction patterns were collected within the 2θ range 0.5–40° using a scanning rate of 0.6°/min. The *d*-spacing was calculated according to Bragg's equation.

Thermogravimetric analyses

The weight loss curves were obtained in a Du Pont Instruments 951 thermogravimetric analyzer. Experiments were made with a 20°/min heating ramp and 50 cm^3/min nitrogen flow within the temperature range 20–800°C.

Scanning electron microscopy

Morphological images were obtained in an Edax scanning electron microscope with Topcon sm-510 detector and a voltage of 15 kV. Samples in this case were prepared from specimens cryogenically fractured. To enhance contrast, the EVA phase of selected samples was extracted with toluene at 40°C for 1 h and then the samples were covered with an ultrathin layer of gold-palladium.

Molecular simulations

Molecular models were designed with the Spartan 04 software and the molecular mechanics force fields algorithm (MMFF) 94 using a HP XW6000 work station. Montmorillonite is natural 2 : 1 clay of the phyllosilicates family. It consists of a stack of layers with 1 nm thickness, formed by a central octahedral sheet of aluminum hydroxide and connected with two external tetrahedral sheets of silica. In this form, the oxygens of the octahedral sheet of aluminum hydroxide also belong to the silica tetrahedral sheets. In their natural form, several aluminum cations are substituted by magnesium cations generating an overall negative charge on the layers surface. The charge is generally compensated by sodium cations or the like.[22] In this form, nanoclay is in a hydrophilic state which makes it incompatible with most of the polymers. Therefore, to enhance compatibility with organic polymers the modification of the hydrophilic surface to the organophilic state is required. Such modification involves cation exchange with organic surfactants such as quaternary alkylammonium ions.[23]

On the basis of the ideal nanoclay structure,[24] in the present study, we have simulated basic nanoclay conformations by assuming a nanolayer with the same length and width (70 nm) and an average thickness of 0.71 nm. The thickness was calculated from the center-to-center distance between the external oxygen atoms of the tetrahedral sheets once the energy was minimized according to

$$\bar{t} = \frac{2\sum_{i=1}^{\frac{n}{2}-m}\left[\left[2(a)^2\right]^{1/2} + 2[b + b\sin\alpha]\right]}{n - 2m} \quad (2)$$

where a is the Al—O bond, b is the Si—O bond, α is the O—Si—O angle, n is the number of oxygen atoms of SiO_4, and m is the number of oxygen atoms of SiO_4 bound to Al. In this form, two layers can be positioned in parallel with the hydrated sodium cations located inside the gallery and the potential energy can be minimized. In the next step the $E_{L\text{-}L}$ (layer–layer) interaction energy, caused by steric effects, is calculated. On the basis of these considerations, the periodicity between layers, d_{001}, was obtained as 11.8 Å. This value is very close to the one that we experimentally obtained, 11.7 Å, for the natural sodium montmorillonite (Cloisite Na^+).

The methyl tallow bis-2-hydroxyethyl, quaternary ammonium organic modifier (Q), attached to the commercial clay Cloisite 30B, was also modeled and theoretically positioned in the interlayer spacing after discarding sodium ions. Once the energy was minimized, the interaction energy, represented as $E_{L\text{-}Q\text{-}L}$ (Layer-Q-Layer), and the repeating distance perpendicular to the layers d_{001} were obtained.

A linear EVA low molecular weight chain was finally considered with molecular weight of 5000 g/g-mol, vinyl acetate (VA) content of 18 wt % (in agreement with the selected EVA), and random position of the vinyl acetate monomers. Once the EVA molecule was introduced within the clay gallery and the energy was minimized, the interaction energy of the system $E_{L\text{-}Q\text{-}EVA\text{-}L}$ (Layer-Q-EVA-Layer) was calculated. This energy was the addition of all possible interactions of the components confined in the interlayer spacing. The periodicity of the layers d_{001} was calculated from the distance between external oxygen atoms of the tetrahedral sheets of the first layer and the internal oxygen atoms of the second layer. Table I shows the calculated *d*-spacing.

TABLE I
Interaction Energies and Interlayer Spacing Obtained from Molecular Models

Molecular model	Interaction energy (Kcal/mol)	*d*-Spacing d_{001} (Å)
$E_{L\text{-}L}$	57127	11.7
$E_{L\text{-}Q\text{-}L}$	48856	15.8
$E_{L\text{-}Q\text{-}EVA\text{-}L}$	48069	20.0

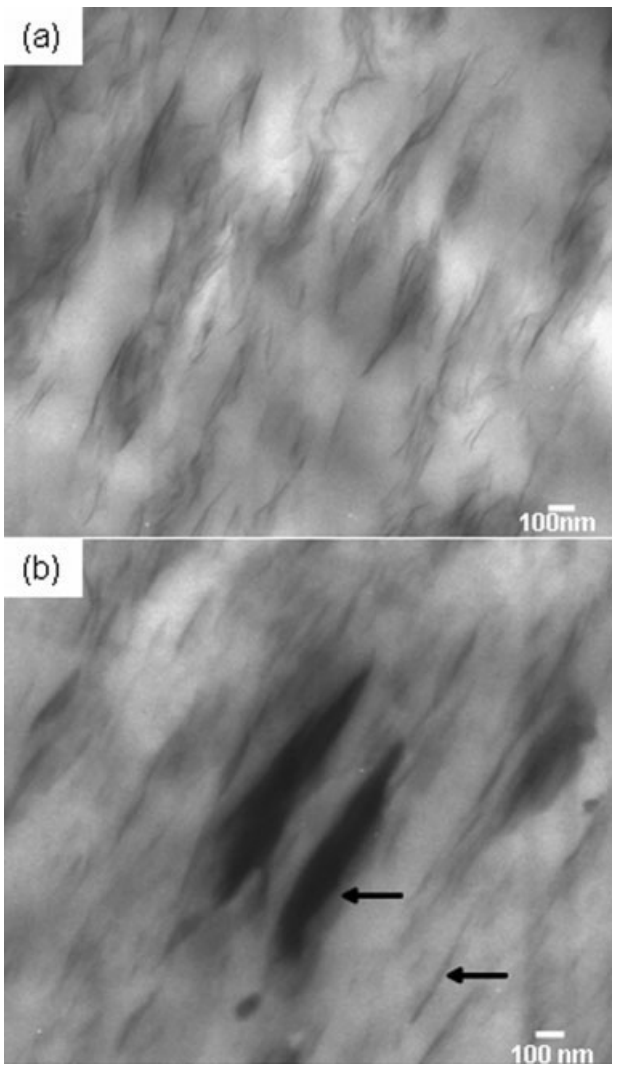

Figure 1 Transmission electron microscopy micrographs of: (a) EVA/Cloisite 20A (8 wt %) and reference Cloisite C20A, and (b) EVA/Cloisite 30B (8 wt %) and reference Cloisite C30B.

RESULTS AND DISCUSSION

Effect of the organic modifier

A number of chemical agents have been used with the purpose to promote nanoclay exfoliation in polymeric nanocomposites. These have included simple surfactant-like molecules and also complex compounds, generally with long tail(s). Figure 1 shows the TEM micrographs of EVA/C20A and EVA/C30B, both with 8 wt % clay. As aforementioned, in C20A and in C30B two and one hydrogenated tallows were used, respectively, to ion exchange the corresponding montmorillonite. The results indicate that important differences originated from the nature of the exchanged chemical groups. For example, in the case of EVA/C20A [Fig. 1(a)] the desired exfoliation of nanolayers, without pronounced formation of clay stacks (i.e., the so called tactoids), is observed. However, in the case of EVA/C30B [Fig. 1(b)] exfoliated nanolayers and also dispersed tactoids characterized the overall morphology (see arrows).

The results in both cases are in agreement with the WAXD patterns shown in Figure 2. Here, the main basal reflection of pure Cloisite C20A [Fig. 2(a)], d_{001}, is observed at $2\theta = 3.7$, although in the mixture EVA/C20A the reflection peak d_{001} appears at $2\theta = 2.3$. The difference is an indication of nanolayers exfoliation in EVA/C20A due to the reciprocal relationship between layer spacing and the position of the reflection peak. On the other hand, when C30B was used in the EVA/C30B mixture [Fig. 2(b)],

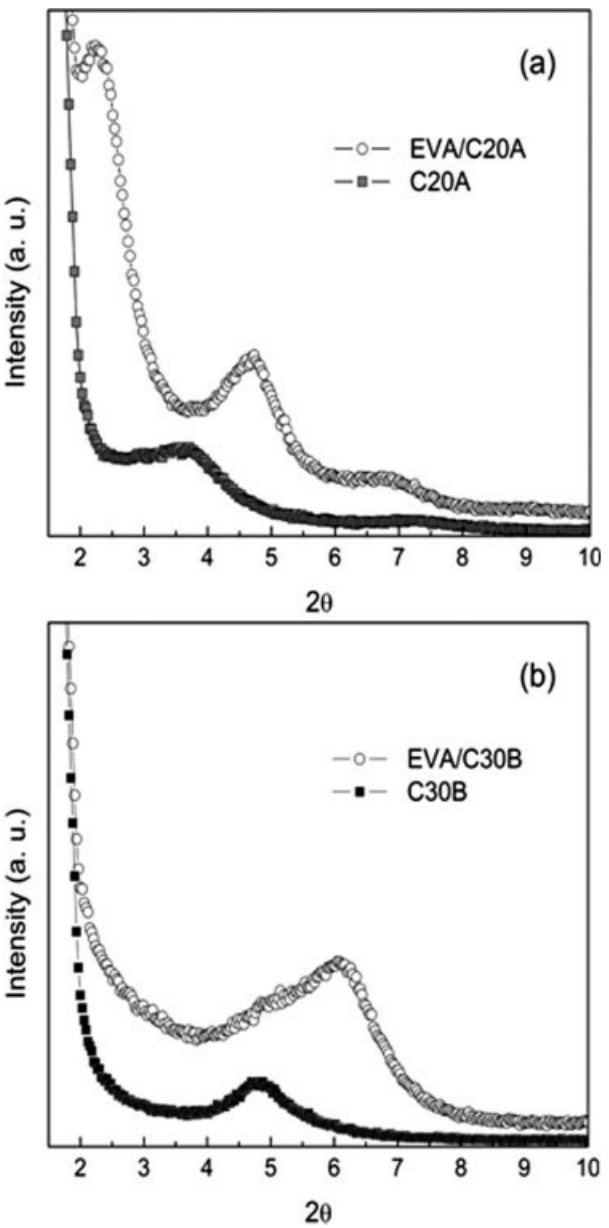

Figure 2 X-ray diffraction patterns of: (a) EVA/Cloisite 20A and (b) EVA/Cloisite 30B both with 8 wt % nanoclay.

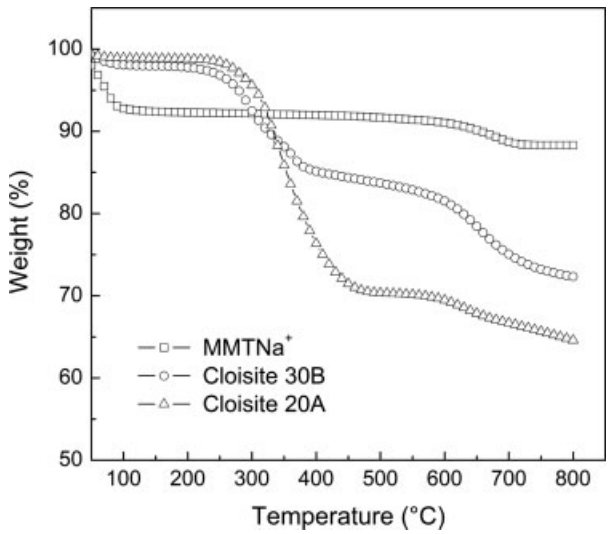

Figure 3 Weight loss curves of montmorillonite without organic modifier ($MMTNa^+$) and organically modified nanoclays (C30B and C20A).

the reflection peak d_{001} was displaced to higher diffracting angles indicating an overall decrease in the layer periodicity. Therefore, these results indicate that the number of hydrogenated tallows dictates in principle the exfoliation properties. However, in addition to the number of hydrogenated tallows, there are some other factors which can affect the nanolayers exfoliation which are addressed in the next paragraphs.

The first possibility is thermal degradation of the organic modifier during melt blending.[16,18] An example is the case studied by Zanetti et al.[18] where a decrease of the interlayer spacing, during extrusion of an EVA copolymer with montmorillonite exchanged with octadecylammonium, was assigned to partial thermal decomposition and volatilization of the organic modifier. Lee et al.[16] also considered the poor thermal stability of Cloisite 30B as the cause of reduction in the interlayer spacing of PP-C30B blends. The TGA results obtained in the present study, and shown in Figure 3, indeed indicate that the thermal decomposition of the organic modifier in Cloisite 30B begins a little earlier than in C20A. However, the results also indicate that thermal degradation of Cloisite 30B begins around 250°C. Therefore, if we consider that the highest extrusion temperature used in the present study was 190°C, thermal degradation of the organic modifier during melt blending can be discarded as the cause of the observed interlayer spacing decrease.

There exists another possibility affecting nanoclay exfoliation, type and nature of molecular interactions between the clay platelets. Two molecular models were used to study this possibility in this work: (i) the confinement of the organic modifier, methyl tallow bis-2-hydroxyethy quaternary ammonium, between two montmorillonite layers [Fig. 4(a)]; and (ii) the confinement of an EVA macromolecule between two organically modified montmorillonite layers [Fig. 4(b)].

Molecular simulations of the confinement of polymers, such as polystyrene[25] and Nylon-6,[26] within silicate layers, have been reported before with a main purpose, to predict the structure of the confined chains and its bonding energies. With this objective, we first focused on predicting the minimum separation length of two modified montmorillonite nanolayers occurring during their structural arrangement until the equilibrium geometry. The resulting *d*-spacing, assuming the organic modifier parallel to the surface of the nanolayers, as shown in Figure 4(a), was 15.8 Å. The experimental *d*-spacing for commercial Cloisite 30B (one hydrogenated tallow), obtained by WAXD, was 18.4 Å. The difference could be taken as an indication that the organic modifier is most probably at an angle respect the horizontal plane of the nanolayers, opening up the nanoclay galleries. A potential cause for the inclination of the modifier is the high concentration of the organic chains that substitute the original exchangeable cations. In support of this proposition, it has been reported before[1] that Cloisites 20A and 15A have the same surfactant modifier although the interlayer spacing is 24.2 and 31.5 Å, respectively. This difference was assigned to both clays having different modifier concentration; Cloisite 20A had 95 mequiv/100 g and C15A 125 mequiv/100 g clay.[27]

The second option, a closer approach to this study, should also consider polar interactions. The organic

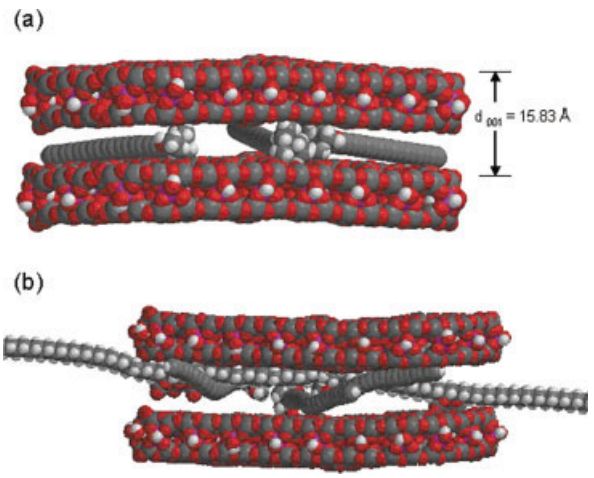

Figure 4 Molecular modeling of (a) confinement of organic modifier (methyl, tallow, bis-2-hydroxyethyl, quaternary ammonium), and (b) additional confinement of an EVA chain within two nanolayers. [Color figure can be viewed in the online issue, which is available at www.interscience.wiley.com.]

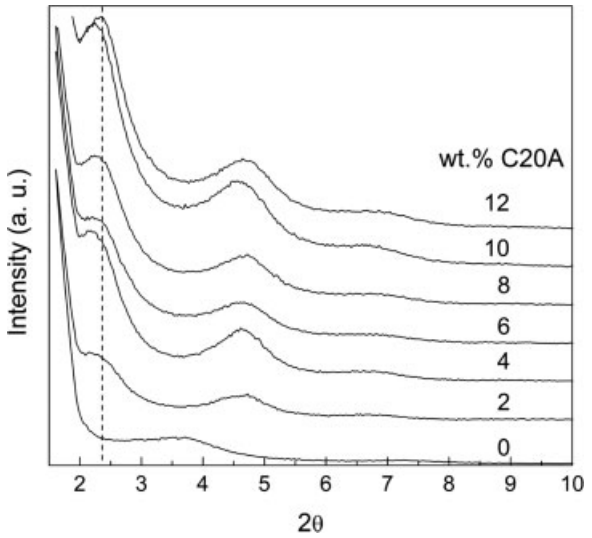

Figure 5 WAXD diffraction patterns of EVA/C20A with the indicated C20A concentrations.

modifier in Cloisite 30B has two polar (CH_2CH_2OH) groups attached to the nitrogen atom, and the single tallow can also be considered polar.[28] These characteristics could influence the interaction with the EVA macromolecules during melt blending which is helped by the high shear stress. In this chemical environment, the partially polar EVA would be able to intercalate between the silicate layers and the periodicity would slightly increase. Figure 4(b) shows the molecular simulation under these hypothetical circumstances when an EVA chain, with 18 wt % vinyl acetate, is allowed to intercalate between the galleries of the organically modified montmorillonite C30B. In this case, the *d*-spacing of the simulation is 20.0 Å, a close value to the one obtained by X-rays (18.4 Å). Such effect however did not take place in practice since there was not experimentally good clay exfoliation in C30B (see for example Fig. 1). Therefore, it can be concluded that the number of tallows must surmount these last molecular interactions, and this is the dominant factor in promoting clay exfoliation.

Effect of nanoclay concentration

Polymeric nanocomposites usually reach a saturated condition at concentrations above 5 wt % due to the high surface area of the clay platelets. Above this saturated condition, nanoclays tend to develop stacks (tactoids).[29,30] Figure 5 shows the X-ray diffraction patterns of the EVA/C20A mixture at concentrations ranging between 2 and 12 wt % clay. In these results, only minor changes of the main reflection, related to the layer–layer periodicity, are observed. Table II shows the results of the interlayer spacing obtained with the different clay concentrations. Contrastingly however, Figure 6 shows a marked change from an exfoliated condition [Fig. 6(a)] for the 2 wt % clay mixture to a mixture of intercalated, exfoliated, and tactoid-like, condition [see arrows in Fig. 6(b)] for the 10 wt % clay mixture. These results are therefore an indication that the WAXD periodicity should be assigned to interlayer spacing within groups of layers (tactoids), rather than to the exfoliated individual layers.

TABLE II
SAXS, Interlayer Spacing of EVA/C20A Mixtures with Different C20A Organoclay Concentrations

C20A (wt %)	*d*-Spacing d_{001} (Å)
2	40.7
4	40.4
6	39.9
8	39.5
10	39.4
12	37.8

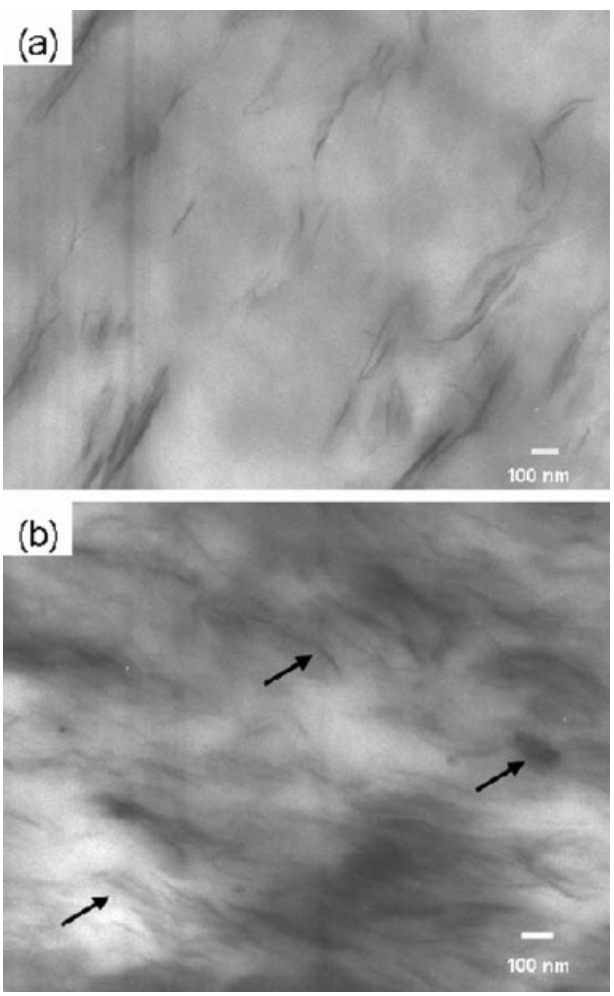

Figure 6 Transmission electron microscopy micrographs of EVA/C20A with: (a) 2 and (b) 10 wt % nanoclay.

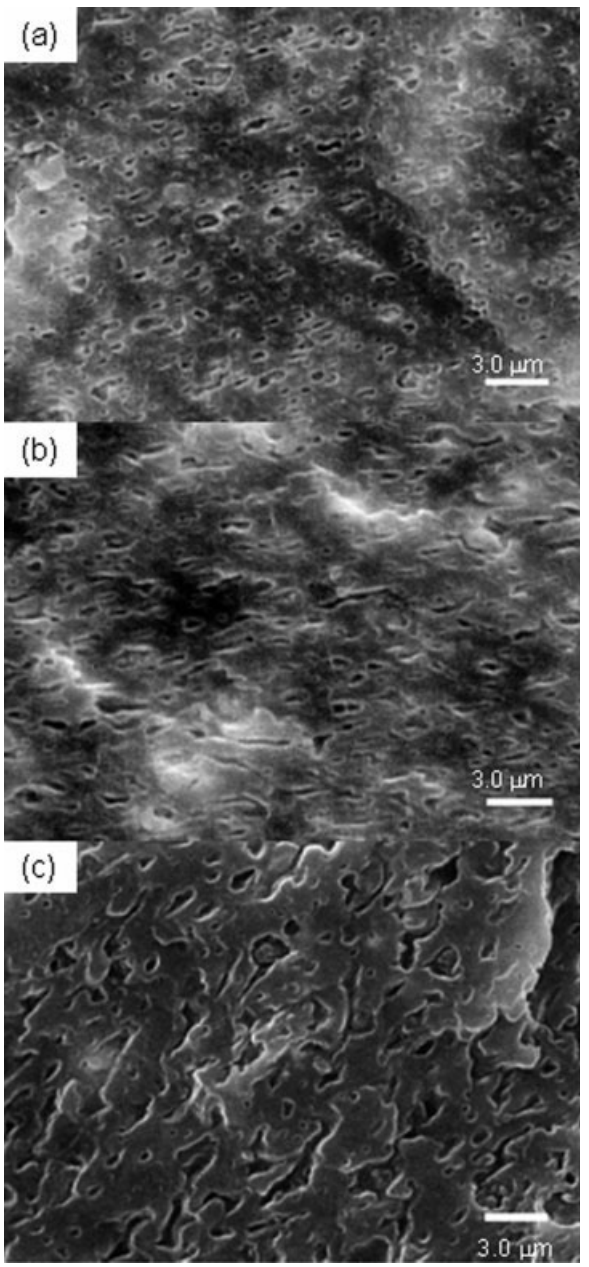

Figure 7 Scanning electron microcopy micrographs of: (a) PP-EP/EVA with 20 wt % EVA, (b) PP-EP/EVA with 40 wt % EVA, and (c) PP-EP/(EVA/C20A) nanocomposite with 40 wt % EVA and 3.2 wt % nanoclay. Samples were extracted with toluene.

Morphological changes

Two immiscible polymers motivate the formation of separated phases since chemical attractions between similar molecules are stronger in each phase. Therefore, immiscibility between the EVA and the PP-EP heterophasic copolymers should generate the formation of two phases during melt blending. This is indeed the case and it is additionally known that PP-EP is the continuous and EVA is the disperse phase in this polymeric system. The disperse phase forms spherical particles or elongated domains depending on its concentration.[31] If the concentration of the disperse phase is high, coalescence occurs and elongated domains are observed. It has been proposed[20] that coalescence can be originated from (1) natural interactions between particles as a consequence of the decrease of the interparticle distance; (2) molecular interactions among the ethylene groups present in both polymers.

Figure 7 shows that coalescence occurs above 20 wt % EVA in the PP-EP/EVA blend since the morphology of the dispersed phase changes from spherical to elongated domains from 20 to 40 wt % EVA [see e.g., Fig. 7(a,b)]. We have previously studied the mechanisms of compatibility between EVA and the complex iPP-EPx heterophasic copolymers as a function of EP,[21] and have previously demonstrated, in terms of glass transition temperatures (T_g) of both copolymers,[20] that the observed change in morphology is associated with a transition toward compatibility of the system. Once nanoclay is introduced under compatibility conditions, the main morphology is preserved, as shown in Figure 7(c) for the PP-EP/EVA (60/40) and 3.2 wt % clay nancomposite. As for the clay platelets location, Figure 8 shows the TEM micrographs of a PP-EP/(EVA/C20A) nanocomposite with 40 wt % EVA and 2.4 wt % C20A. As indicated with an arrow, it is observed that the silicate layers actually reside inside the EVA domains. These results are in agreement with the WAXD patterns of the same sample, shown in Figure 9, after toluene extraction of the EVA phase. Here, it is observed that the reflection peak corresponding to the interlayer distance (d_{001}) is not present anymore. There are additional features in the diffraction patterns indicating the evolution of other

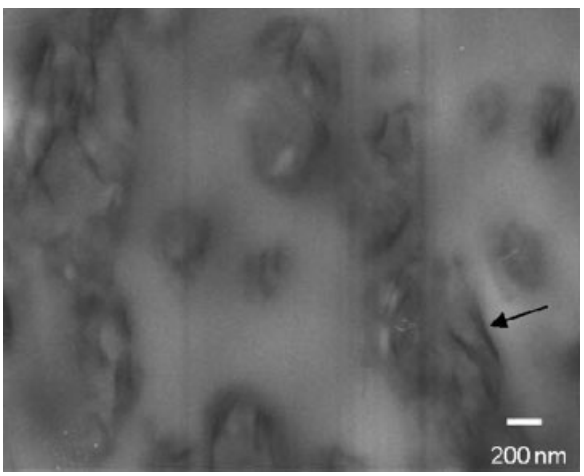

Figure 8 Transmission electron micrograph of PP-EP/(EVA/C20A) nanocomposite with 40 wt % EVA and 2.4 wt % nanoclay. Arrow shows nanoclay aggregate within the EVA domains.

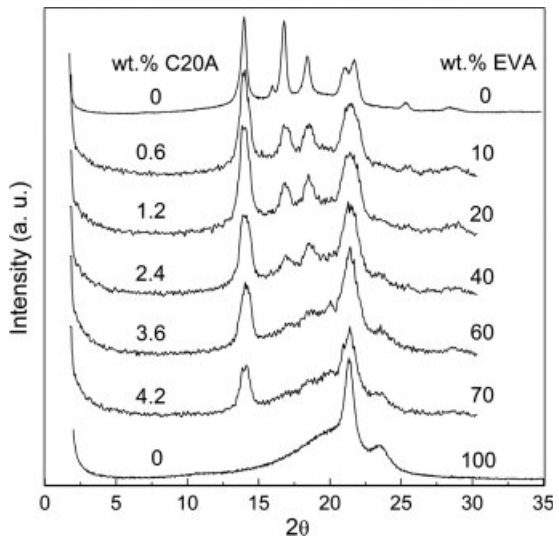

Figure 9 WAXD patterns of the PP-EP/(EVA/C20A) system after extraction with toluene, the EVA and nanoclay concentrations are indicated.

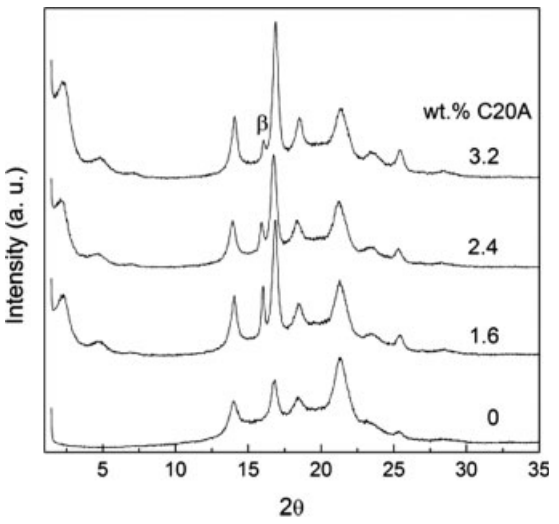

Figure 11 WAXD patterns of PP-EP/(EVA/C20A) nanocomposites with 40 wt % EVA and the indicated nanoclay concentrations.

morphologies. These might include nonextractable EVA and extractable PP-EP. The analysis of these changes is however not the purpose of the present study.

Crystal structures evolution

Several studies[32–36] have reported the effect of nanoclays on the crystallization habits of polymers. For example, it has been determined that γ crystals are preferentially formed in the presence of nanoclay in Nylon 6 nanocomposites.[32–34] This crystal form has also been obtained in iPP nanocomposites.[35,36] Figure 10 shows the WAXD results of the studied PP-EP/EVA blends. In the case of the neat PP-EP heterophasic copolymer, the diffraction peaks, which correspond to the α crystalline form, are located at 2θ values of 14.1, 16.9, 18.6, 21.2, and 21.9°. The one corresponding to the β crystalline form (which is not formed in any case) should be located at 2θ = 16.11°. The EVA copolymer on the other hand shows a simple reflection peak at 2θ = 21° assigned to the polyethylene part in the copolymer. In general, the results indicate a gradual evolution of the original crystalline structures toward the other, depending on composition. They also show that EVA does not promote the β crystal habit at any concentration.

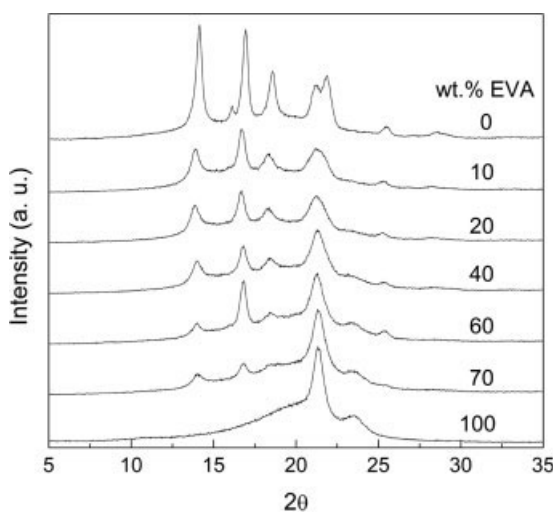

Figure 10 WAXD patterns of the PP-EP/EVA blend with different EVA concentrations.

In the case of ternary nanocomposites PP-EP/(EVA/C20A) (40 wt % EVA), whose results are shown in Figure 11, there appears the diffraction peak associated with nanoclay at low diffracting angles and there is also an inverse relationship between the formation of β crystals and the nanoclay content. This inverse relationship between the formation of β crystals and the nanoclay content is related to the amount of truly exfoliated single platelets, as reported in a separate study.[37]

CONCLUSIONS

The number of organic modifier influences nanoclay integration in PP-EP/EVA/nanoclay nanocomposites. Two hydrogenated tallows are better than one in promoting nanoclay exfoliation.

Thermal degradation of the organic modifier during melt blending of the mixture was discarded as a potential cause of exfoliation decrease in these studies.

Molecular simulations indicated that the organic modifier is most probably at an angle respect the

horizontal plane of the nanolayers, opening up the nanoclay galleries. The simulations also indicated that the polar nature of the organic modifier does not have a major impact in exfoliation properties.

The introduction of nanoclay in the PP-EP/EVA system, under compatibility conditions, preserved the original domains-type morphology. It was also determined that the silicate layers are hosted by the EVA domains.

The crystallization characteristics of the PP-EP/EVA mixtures indicated a gradual evolution of the corresponding crystalline structures depending on the EVA content. In the case of the ternary nanocomposites, the β crystalline structure decreased with increasing nanoclay content.

The authors thank Josefina Zamora-Rodríguez for the preparation of the ultra-thin cryogenic samples, and Myriam Lozano Estrada for the thermal and WAXD characterizations.

References

1. Fornes, T. D.; Yoon, P. J.; Hunter, D. L.; Keskkula, H.; Paul, D. R. Polymer 2002, 43, 5915.
2. Zhang, W.; Chen, D.; Zhao, Q.; Fang, Y. Polymer 2003, 44, 7953.
3. Fornes, T. D.; Hunter, D. L.; Paul, D. R. Macromolecules 2004, 37, 1793.
4. Kawasumi, M.; Hasegawa, N.; Kato, M.; Usuki, A.; Okada, A. Macromolecules 1997, 30, 6333.
5. García-López, D.; Picazo, O.; Merino, J. C.; Pastor, J. M. Eur Polym J 2003, 39, 945.
6. Liu, X.; Wu, Q. Polymer 2001, 42, 10013.
7. Manias, E.; Touny, A.; Wu, L.; Strawhecker, K.; Lu, B.; Chung, T. C. Chem Mater 2001, 13, 3516.
8. Ristolainen, N.; Vainio, U.; Paavola, S.; Torkkeli, M.; Serimaa, R.; Sépala, J. J Polym Sci Part B: Polym Phys 2005, 43, 1892.
9. Mani, G.; Fan, Q.; Ugbolue, S. C.; Yang, Y. J Appl Polym Sci 2005, 97, 218.
10. Gahleitner, M.; Kretzschmar, B.; Pospiech, D.; Ingolic, E.; Reichelt, N.; Bernreitner, K. J Appl Polym Sci 2006, 100, 283.
11. Alexandre, M.; Beyer, G.; Henrist, C.; Cloots, R.; Rulmont, A.; Jérôme, R.; Dubois, P. Macromol Rapid Commun 2001, 22, 643.
12. Riva, A.; Zanetti, M.; Braglia, M.; Camino, G.; Falqui, L. Polym Degrad Stab 2002, 77, 299.
13. Tang, Y.; Hu, Y.; Wang, S. F.; Gui, Z.; Chen, Z.; Fan, W. C. Polym Degrad Stab 2002, 78, 555.
14. Chaudhary, D. S.; Prasad, R.; Gupta, R. K.; Bhattacharya, S. N. Polym Eng Sci 2005, 45, 889.
15. Peeterbroeck, S.; Alexandre, M.; Jérôme, R.; Dubois, P. Polym Degrad Stab 2005, 90, 288.
16. Lee, J. W.; Lim, Y. T.; Park, O. O. Polym Bull 2000, 45, 191.
17. Li, X.; Ha, C. S. J Appl Polym Sci 2003, 87, 1901.
18. Zanetti, M.; Camino, G.; Thomann, R.; Mülhaupt, R. Polymer 2001, 42, 4501.
19. Valera-Zaragoza, M.; Ramírez-Vargas, E.; Medellín-Rodríguez, F. J.; Huerta-Martínez, B. M. Polym Degrad Stab 2006, 91, 1319.
20. Ramírez-Vargas, E.; Medellín-Rodríguez, F. J.; Navarro-Rodríguez, D.; Avila-Orta, C. A.; Solís-Rosales, S. G; Lin, J. S. Polym Eng Sci 2002, 42, 1350.
21. Huerta-Martínez, B. M.; Ramírez-Vargas, E.; Medellín-Rodríguez, F. J.; Cedillo-García, R. Eur Polym J 2005, 41, 519.
22. Manias, E. Advances in Fire Retardant Chemicals, FRCA; DEStech Publications: Lancaster, PA, 2002.
23. Giannelis, E. P.; Krishnamoorti, R. K.; Manias, E. Adv Polym Sci 1998, 138, 107.
24. Shriver, D. F.; Atkins, P. W.; Langford, C. H. In Inorganic Chemistry, 2nd ed.; W. H. Freeman & Co., Ltd: New York, 1994; p 1153.
25. Manias, E.; Kuppa, V. In Polymer Nanocomposites: Synthesis, Characterization, and Modeling; Krishnamoorti, R., Vaia, R. A., Eds.; American Chemical Society: Washington, DC, 2002; ACS Symposium Series 804; p 193.
26. Tanaka, G.; Goettler, L. A. Polymer 2002, 43, 541.
27. www.scprod.com and www.nanoclay.com, Product Bulletin/ Cloisite®. Rockwood Additives, Gonzales, TX, 2003.
28. Friedli, F. E. In Cationic Surfactants: Organic Chemistry; Richmond, J. M., Ed.; Marcel Dekker: New York, 1990; p 84, Surfactant Science Series 34.
29. Koo, C. M.; Kim, S. O.; Chung, I. J. Macromolecules 2003, 36, 2748.
30. Chen, L.; Wong, S. C.; Pisharath, S. J Appl Polym Sci 2003, 88, 3298.
31. Thomas, S.; George, A. Eur Polym J 1992, 28, 1451.
32. Fornes, T. D.; Paul, D. R. Polymer 2003, 44, 3945.
33. Medellín-Rodríguez, F. J.; Burger, C.; Hsiao, B. S.; Chu, B.; Vaia, R.; Phillips, S. Polymer 2001, 42, 9015.
34. Zapata-Espinosa, A.; Medellín-Rodríguez, F. J.; Stribeck, N.; Almendarez-Camarillo, A.; Vega-Díaz, S.; Hsiao, B. S.; Chu, B. Macromolecules 2005, 38, 4246.
35. Nam, P. H.; Maiti, P.; Okamoto, M.; Kotaka, T.; Hasegawa, N.; Usuki, A. Polymer 2001, 42, 9633.
36. Maiti, P.; Nam, P. H.; Okamoto, M.; Kotaka, T.; Hasegawa, N.; Usuki, A. Polym Eng Sci 2002, 42, 1864.
37. Medellín-Rodríguez, F. J.; Mata-Padilla, M.; Hsiao, B.; Ramirez-Vargas, E.; Sanchez-Valdes, S. Polym Sci Eng, to appear.